







Communication

# Highly Sensitive Electrochemical Non-Enzymatic Uric Acid Sensor Based on Cobalt Oxide Puffy Balls-like Nanostructure

Vandana Nagal <sup>1,†</sup>, Sakeena Masrat <sup>1,†</sup>, Marya Khan <sup>1</sup>, Shamshad Alam <sup>2</sup>, Akil Ahmad <sup>3</sup>, Mohammed B. Alshammari <sup>3</sup>, Kiesar Sideeq Bhat <sup>4,5</sup>, Sergey M. Novikov <sup>6</sup>, Prabhash Mishra <sup>1</sup>, Ajit Khosla <sup>7,\*</sup> and Rafiq Ahmad <sup>1,\*</sup>

<sup>1</sup> Centre for Nanoscience and Nanotechnology, Jamia Millia Islamia, New Delhi 110025, India

<sup>2</sup> Department of Pharmacology & Therapeutics, Rosewell Park Cancer Institute, Elm Street & Carlton Street, Buffalo, NY 14263, USA

<sup>3</sup> Department of Chemistry, College of Science and Humanities in Al-Kharj, Prince Sattam Bin Abdulaziz University, Al-Kharj 11942, Saudi Arabia

<sup>4</sup> Department of Bioresources, University of Kashmir, Hazratbal, Srinagar 190006, India

<sup>5</sup> Singapore-MIT Alliance for Research and Technology (SMART), Critical Analytics for Manufacturing Personalized-Medicine (CAMP), Create Way 138602, Singapore

<sup>6</sup> Center for Photonics and 2D Materials, Moscow Institute of Physics and Technology, Dolgoprudny 141700, Russia

<sup>7</sup> Department of Applied Chemistry, School of Advanced Materials and Nanotechnology, Xidian University, Xi'an 710126, China

\* Correspondence: ajitkhosla@xidian.edu.cn (A.K.); rahmad5@jmi.ac.in (R.A.)

† These authors contributed equally to this work.

**Abstract:** Early-stage uric acid (UA) abnormality detection is crucial for a healthy human. With the evolution of nanoscience, metal oxide nanostructure-based sensors have become a potential candidate for health monitoring due to their low-cost, easy-to-handle, and portability. Herein, we demonstrate the synthesis of puffy balls-like cobalt oxide nanostructure using a hydrothermal method and utilize them to modify the working electrode for non-enzymatic electrochemical sensor fabrication. The non-enzymatic electrochemical sensor was utilized for UA determination using cyclic voltammetry (CV) and differential pulse voltammetry (DPV). The puffy balls-shaped cobalt oxide nanostructure-modified glassy carbon (GC) electrode exhibited excellent electro-catalytic activity during UA detection. Interestingly, when we compared the sensitivity of non-enzymatic electrochemical UA sensors, the DPV technique resulted in high sensitivity (2158  $\mu\text{A}/\text{mM}\cdot\text{cm}^2$ ) compared to the CV technique (sensitivity = 307  $\mu\text{A}/\text{mM}\cdot\text{cm}^2$ ). The developed non-enzymatic electrochemical UA sensor showed good selectivity, stability, reproducibility, and applicability in the human serum. Moreover, this study indicates that the puffy balls-shaped cobalt oxide nanostructure can be utilized as electrode material for designing (bio)sensors to detect a specific analyte.

**Keywords:** cobalt oxide; puffy balls nanostructure; cyclic voltammetry; high sensitivity; uric acid; differential pulse voltammetry



**Citation:** Nagal, V.; Masrat, S.; Khan, M.; Alam, S.; Ahmad, A.; Alshammari, M.B.; Bhat, K.S.; Novikov, S.M.; Mishra, P.; Khosla, A.; et al. Highly Sensitive Electrochemical Non-Enzymatic Uric Acid Sensor Based on Cobalt Oxide Puffy Balls-like Nanostructure. *Biosensors* **2023**, *13*, 375. <https://doi.org/10.3390/bios13030375>

Received: 3 February 2023

Revised: 6 March 2023

Accepted: 11 March 2023

Published: 12 March 2023



**Copyright:** © 2023 by the authors. Licensee MDPI, Basel, Switzerland. This article is an open access article distributed under the terms and conditions of the Creative Commons Attribution (CC BY) license (<https://creativecommons.org/licenses/by/4.0/>).

## 1. Introduction

Uric acid (UA) is a waste product in human fluids (i.e., blood and urine). It is produced when the chemical known as purine nucleotides (natural substances present in the body) is broken down by the body. The normal ranges of uric acid in urine and serum for healthy individuals are 1.40–4.40 mM and 0.30–0.50 mM, respectively [1]. The abnormal presence of UA concentration in the body is harmful [2–4]. When the UA concentration in the blood increases from the normal level, it causes diseases like gout and other related ailments, such as tumor lysis syndrome, diabetes, uric acid stone formation, and many more. On the other hand, a decrease in UA concentration from the normal level leads to hypouricemia,

which in turn leads to chronic kidney failure, multiple sclerosis, etc. [5–7]. Therefore, early diagnosis of abnormal UA levels is necessary to prevent certain health issues.

Several standard methods are available for UA detection, like mass spectrometry/chromatography, electrochemical enzymatic/non-enzymatic technique, and phosphotungstic acid reduction [8–12]. Mass spectrometry/chromatography is a suitable choice because of its high sensitivity and good reliability, but the major drawback of this method is the high cost of the instrument. The reduction of phosphotungstic acid is a simple and easy approach compared to other methods, but its operation is restricted due to interference effects. Therefore, electrochemical sensing approaches are preferred over other methods in analytical chemistry for the accurate quantitative estimation of parameters like sensitivity, selectivity, and responsiveness. In addition, these electrochemical sensors offer small size, minimum cost, long-term sustainability/storage, reliability, and eco-friendliness as important factors [13–15]. On the other hand, the electrochemical enzyme-based sensors are highly specific but not a good choice because of their complicated enzyme immobilization techniques, high enzyme costs, low repeatability rate, long-term storage/stability issues, and severe operating conditions [16–18]. Therefore, the researcher's focus has switched towards non-enzymatic electrochemical sensing devices that utilize special properties of metal/metal oxide nanostructures [19–21]. The non-enzymatic sensors, when fabricated with desired metal/metal oxide nanostructures, show exceptional capability and sensing performance for detecting analytes like glucose, ascorbic acid, dopamine, hydrazine, uric acid, etc. [22–28].

The metal oxide nanomaterials (e.g., zinc oxide (ZnO), nickel oxide (NiO<sub>x</sub>), manganese oxide (Mg<sub>2</sub>O), zirconium oxide (Zr<sub>2</sub>O), iron oxide (Fe<sub>2</sub>O<sub>3</sub>), and cobalt oxide (Co<sub>3</sub>O<sub>4</sub>))-based electrochemical sensors are catching the interest of researchers due to their extraordinary physical properties like reliability, stability, small packaging, and minimum cost [29–34]. Nanostructures of cobalt oxide are being used to construct non-enzymatic electrochemical sensors due to simple and low-cost synthesis processes, chemical stability, and fast charge transfer property [29,30,35]. Recently, nano-berry, porous, and hexagonal nanosheet-like nanostructures of cobalt oxides were utilized to fabricate non-enzymatic UA sensors [36–38]. Kogularasu et al. synthesized polyhedron-shaped Co<sub>3</sub>O<sub>4</sub> nanostructures to construct a high-sensitivity hydrogen peroxide sensor [39]. Zhang et al. described the effect of Co<sub>3</sub>O<sub>4</sub> nanosheets on enzymeless glucose detection [40]. Kang et al. investigated the effect of nanowire shapes like Co<sub>3</sub>O<sub>4</sub> nanostructures on the glucose sensor [41]. Mondal et al. reported an enzymeless glucose sensor by utilizing various nanostructures of Co<sub>3</sub>O<sub>4</sub> (i.e., nanoflowers, porous nanorods, and spherical nanoparticles) [42]. Chang et al. employed several structures of Co<sub>3</sub>O<sub>4</sub>, for example, nanowire, lump, and flower-like morphologies, to detect lactic acid [43]. However, till now, there are no reports on puffy balls-shaped Co<sub>3</sub>O<sub>4</sub> nanostructures based on non-enzymatic electrochemical UA sensing.

In this work, we designed a non-enzymatic electrochemical UA sensor using puffy balls-like cobalt oxide nanostructure. First, puffy balls-like cobalt oxide nanostructures were synthesized using a low-cost hydrothermal method and characterized with different techniques for structural and morphological analysis. Then, the non-enzymatic electrochemical UA sensor (cobalt oxide puffy balls/GCE) was fabricated, and the sensing activity of the as-prepared nanostructured-based sensor was investigated using electrochemical techniques (i.e., CV, electrochemical impedance spectroscopy (EIS), and DPV). The cobalt oxide puffy balls/GCE sensor using the DPV technique exhibited excellent sensitivity (2158 μA/mM.cm<sup>2</sup>) towards UA detection. In addition, selectivity, stability, reproducibility, and UA detection in human serum were conducted to establish the feasibility of the sensor for future applications.

## 2. Materials and Methods

### 2.1. Chemicals

Cobalt nitrate hexahydrate (purity ≥ 99.99%, Co(NO<sub>3</sub>)<sub>2</sub>.6H<sub>2</sub>O), urea (purity 99%), ethanol (laboratory reagent), 2-(2-Butoxyethoxy) ethyl acetate (purity ≥ 99.2%, binder),

uric acid (purity  $\geq 99\%$ ), potassium chloride (KCl), sodium chloride (NaCl), potassium hexacyanoferrate (purity  $\geq 99\%$ ,  $K_3[Fe(CN)_6]$ ), and phosphate buffer saline (pH = 7.4, PBS) solution were purchased from Sigma-Aldrich. All analytical grade chemicals were used for this work.

### 2.2. Synthesis of Puffy Balls-like Cobalt Oxide Nanostructures

A low-cost and low-temperature hydrothermal method has been utilized for the growth of puffy balls-shaped cobalt oxide nanostructures. Precisely, 1.45 g of cobalt nitrate hexahydrate and urea were dissolved separately in 20 mL of DI water. Both prepared solutions were thoroughly mixed (total 40 mL) using magnetic stirring for 10 min at 450 rpm. The as-prepared homogeneous solution was poured into a stainless-steel lined autoclave and maintained at 150 °C for 4 h. When the autoclave was cooled to room temperature, the black solution was washed using ethanol and DI water to remove the impurities. After washing, the black precipitate sample was vacuum dried at 60 °C for 24 h. In the end, the black powder sample was vacuum annealed at 500 °C for 3 h at a ramp rate of 10 °C/minute before characterization.

### 2.3. Non-Enzymatic Electrochemical UA Sensor Fabrication

To fabricate a non-enzymatic electrochemical UA sensor, the GC electrode was first polished and then cleaned using ultrasonication several times in nitric acid, ethanol, and DI water. Then, a slurry of puffy balls-shaped cobalt oxide nanostructure (0.02 g) was prepared in 100  $\mu$ L binder (2-(2-Butoxyethoxy) ethyl acetate) with the help of ultrasonication for 10 min to get a uniform suspension. Further, an optimized 6  $\mu$ L slurry was drop-casted onto the working GC electrode and kept for drying in the oven for 6 h. A detailed sensor fabrication procedure is shown in Figure 1.

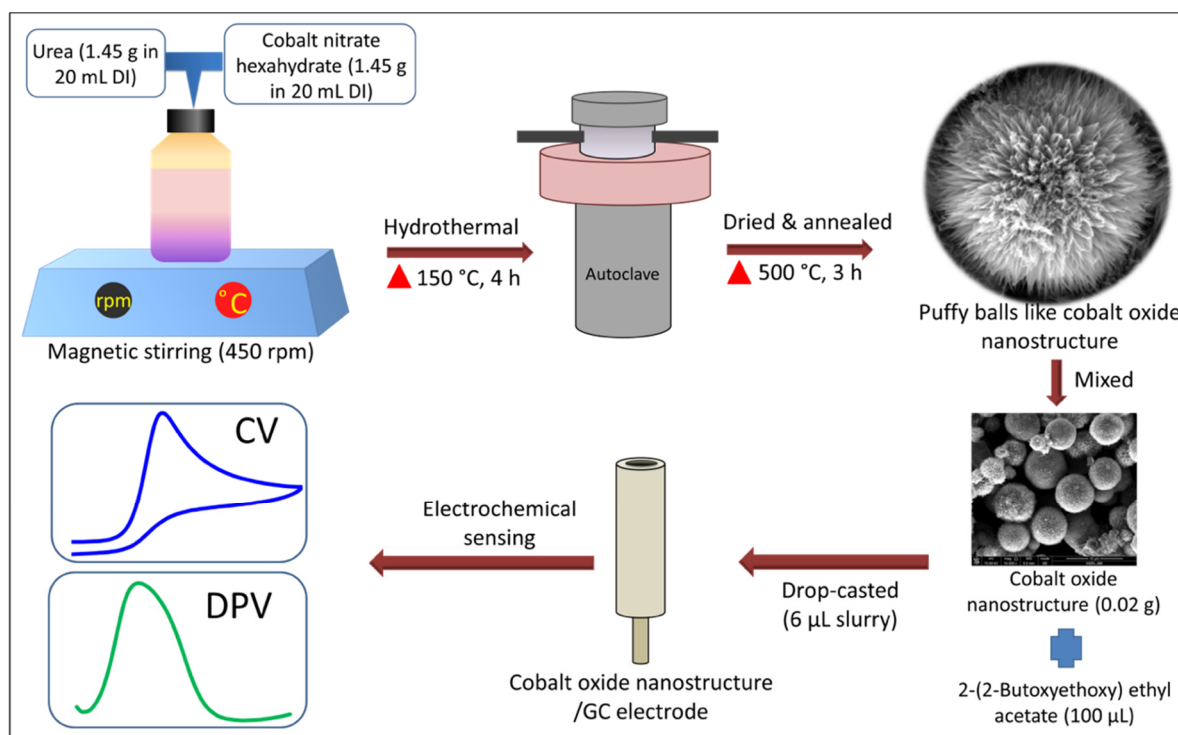


**Figure 1.** Schematic representation of puffy balls-like cobalt oxide nanostructures synthesis and non-enzymatic electrochemical UA sensor fabrication process.

#### 2.4. Material Characterization and Electrochemical Sensing Analysis Equipment

The field-emission-scanning-electron-microscope (FESEM; Zeiss, Oberkochen, Germany) was used to characterize the morphology of the puffy balls-shaped cobalt oxide nanostructure. The crystal structure and phase purity integrity were characterized using an X-ray diffractometer (XRD; Rigaku). XRD machine was equipped with Cu-K $\alpha$  radiation source of wavelength (1.5418 Å), operating voltage (40 kV), and current (30 mA). The ASAP 2010 analyzer was utilized for BET (Brunauer–Emmett–Teller) analysis at 77 K. The UA electrochemical sensing ability of fabricated cobalt oxide puffy balls/GC non-enzymatic electrochemical UA sensor was tested via a portable potentiostat “PalmSense4” connected with a conventional 3-electrode (working (GC), counter (Pt wire), reference (Ag/AgCl, 3M KCl)) electrochemical workstation. The electrochemical analysis was performed using EIS, CV, and DPV measurements. We utilized the previously optimized cobalt oxide amount and pH to get the optimum sensing response of the fabricated sensor [36–38]. The CV was performed in a 5 mM probe solution of potassium hexacyanoferrate (purity  $\geq 9\%$ , K $_3$ [Fe(CN) $_6$ ]) in 0.1 M KCl under varying scan rates from 10 mVs $^{-1}$  to 200 mVs $^{-1}$ . The EIS was studied in the frequency range of 0.1 to 10 $^{-5}$  Hz. The UA analyte sensing was performed using CV (voltage range =  $-0.20$  V to  $+0.80$  V) and DPV (voltage range =  $+0.20$  V to  $+0.70$  V).

### 3. Results

#### 3.1. Analysis of Cobalt Oxide Nanostructure

The morphology of synthesized cobalt oxide nanostructures is shown in FESEM images (Figure 2a–c), which depicts the successful formation of puffy balls-like cobalt oxide nanostructures. These nanostructures are synthesized in uniform shape, evident from the low-magnification FESEM image, shown in Figure 2a. The high-resolution FESEM image shows many pine needle-like nanostructures joined at the top to form a chrysanthemum-like hierarchical structure (Figure 2c). The energy-dispersive X-ray (EDX) analysis confirms this.

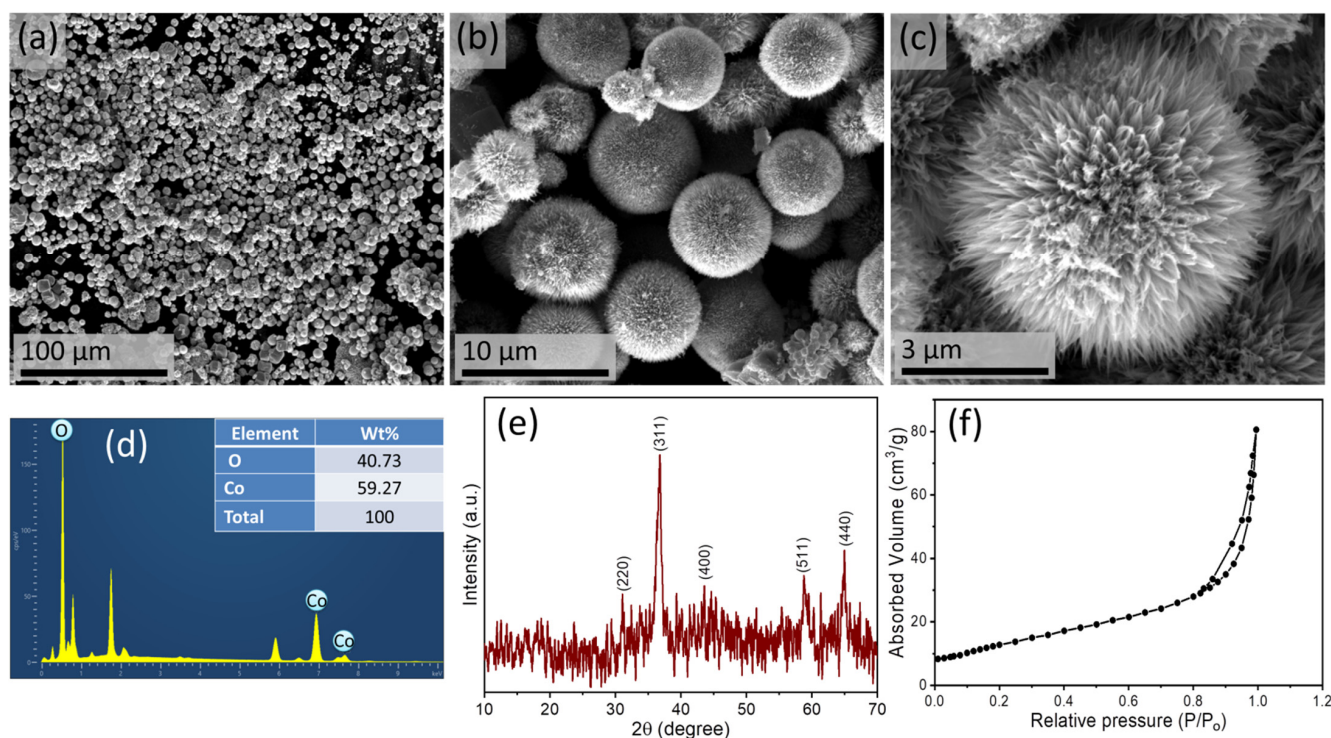


**Figure 2.** FESEM images at different magnifications (a–c), EDX analysis (d), XRD pattern (e), and BET analysis (f) of puffy balls-like cobalt oxide nanostructure.

The composition of puffy balls-like cobalt oxide nanostructure (Figure 2d). The EDX shows only two elements (i.e., oxygen and cobalt). Further, the XRD pattern was investigated to study the crystallinity and crystal phase of puffy balls-like cobalt oxide nanostructures, as shown in Figure 2e. The synthesized crystal structure and obtained diffraction peaks are in good agreement with standard JCPDS card# 42-1467 [39,42]. The different diffraction ( $2\theta$  values) planes with corresponding miller indices (220), (311), (400), (511), and (440) were obtained. A clear peak for the (311) plane is of the highest intensity, indicating the crystalline nature of synthesized cobalt oxide nanostructures [44]. Additionally, we analyzed the surface area of the cobalt oxide puffy balls-like nanostructure using BET analysis (Figure 2f). The specific surface area was  $\sim 93 \text{ m}^2/\text{g}$ , which suggests cobalt oxide puffy balls-like nanostructures are suitable nanomaterials as high-performance catalysts.

### 3.2. Electrochemical Sensing Analysis of Cobalt Oxide Puffy Balls/GC Electrodes

The EIS and CV studies were performed in the potassium hexacyanoferrate ( $\text{K}_3[\text{Fe}(\text{CN})_6]$ ; 5 mM) and 0.1 M KCl solution to investigate the electron transfer capability of the puffy balls-shaped cobalt oxide nanostructure-modified sensor electrode. The Nyquist plots of obtained EIS spectra profile for bare GC and cobalt oxide puffy balls/GC electrodes (Figure 3). The Nyquist plot has a semicircle in a high-frequency region corresponding to the charge transfer-controlled process and a straight line corresponding to the mass transfer diffusion-controlled process. The charge transfer resistance value was determined by the semicircle diameter intercept value on the x-axis. The calculated charge transfer resistance for bare GC electrode ( $\sim 2230 \Omega$ ) is higher compared to cobalt oxide puffy balls/GC electrode ( $\sim 980 \Omega$ ), indicating better charge transfer capabilities of cobalt oxide puffy balls nanostructures.

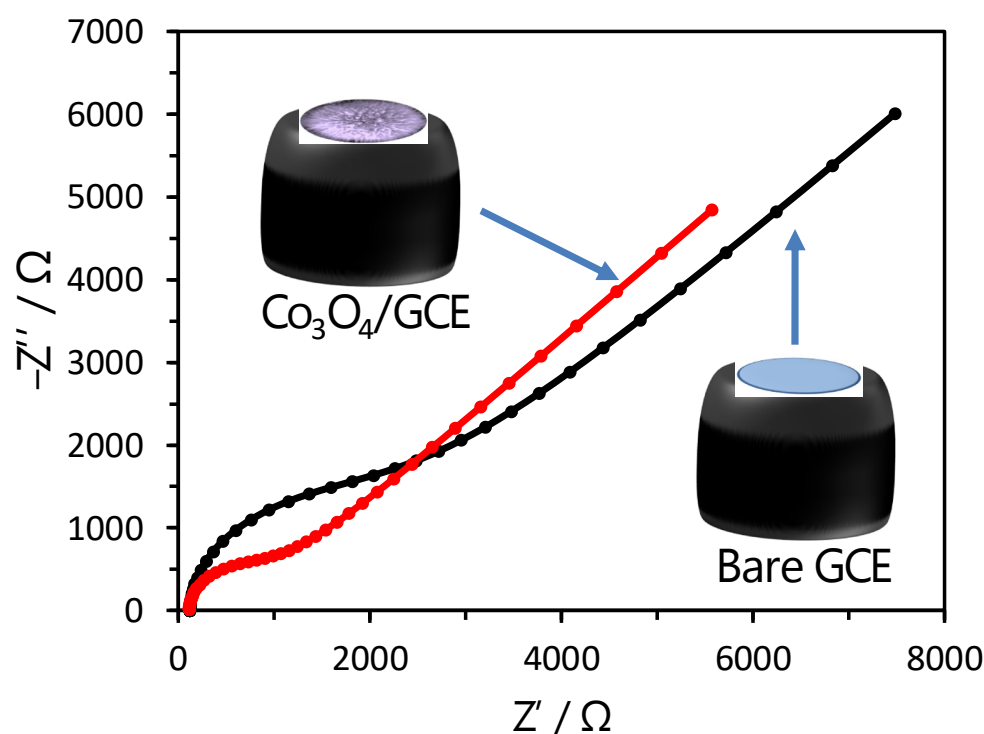


**Figure 3.** Nyquist plots of bare GC and cobalt oxide puffy balls/GC sensors in probe solution (5 mM,  $\text{K}_3[\text{Fe}(\text{CN})_6]$  and 0.1 M KCl); frequency range = 0.1 Hz to  $10^{-5}$  Hz. Insets show the schemes of bare (above inset) and modified (below inset) GC electrodes.

To further validate the electron transfer of cobalt oxide puffy balls/GC electrodes, the CV response was measured at varying scan rates (10 to  $200 \text{ mVs}^{-1}$ ) (Figure 4). The CV response shows the increase in peak current with an increasing scan rate. This increase

is linear when drawing a plot for anodic/cathodic current vs. square root of scan rate plot (inset of Figure 4). The cobalt oxide puffy balls/GC electrodes showed a typical diffusion-controlled process for the reversible system [36]. Both CV and EIS measurements in the probe solution confirm the fast electron transfer capability of cobalt oxide puffy balls/GC electrode.

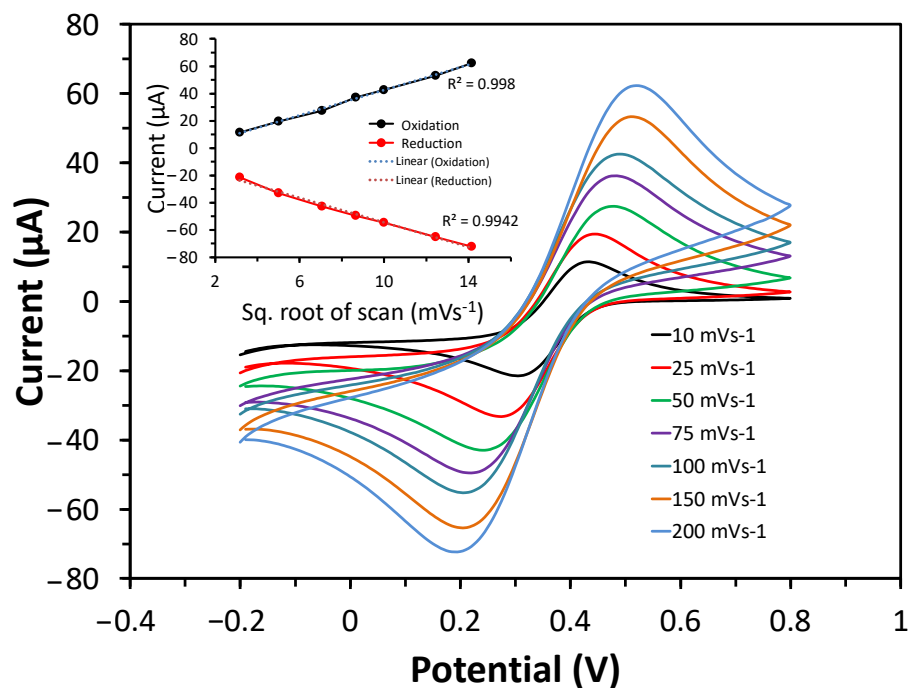


**Figure 4.** CV curve of cobalt oxide puffy balls nanostructures/GC electrode measured in probe solution from 10 to 200 mVs<sup>-1</sup> scan rates. Inset shows the anodic/cathodic current vs. square root of the scan rate plot.

### 3.3. Detection of UA Using CV

To investigate the electrochemical non-enzymatic sensing of fabricated cobalt oxide puffy balls/GC sensor, the CV response was measured in PBS buffer solution (pH = 7.4) having UA at 50 mVs<sup>-1</sup> scan rate. Figure 5a depicts the CV response curve of the cobalt oxide puffy balls/GC sensor for 0 mM and 25 mM UA concentrations. A sharp increase in current response is seen in the presence of UA due to the UA oxidation, where the p-type nature of the cobalt oxide semiconductor plays a crucial role in swift electron transfer to the electrode surface by providing excess hole concentration [30,36,37]. A detailed UA sensing mechanism over cobalt oxide is proposed by Hu et al. [45]. Furthermore, a detailed study of the sensor performance was conducted by measuring UA concentrations from 0 µM to 1500 µM in PBS buffer solution (Figure 5b). With increasing UA concentration in the buffer solution, the non-enzymatic cobalt oxide puffy balls/GC sensor showed an enhanced current response. The peak current vs. UA concentration plot is plotted in Figure 5c, which shows a linear current increase up to 1000 µM of UA. Further increase in UA concentration shows a non-linear curve due to saturation of the cobalt oxide puffy balls/GC sensor surface. Similarly, we repeated these electrochemical non-enzymatic sensing experiments three times, and their calibration plot of the linear range is plotted in Figure 5d. The calibration plot shows the slope of 0.0263 µA/µM with high regression coefficient (R<sup>2</sup>) of 0.9907. The fabricated cobalt oxide puffy balls/GC sensor exhibited a sensitivity of 370 µA/mM.cm<sup>2</sup>. Additionally, the limit of detection was calculated to be 2.4 µM based on the signal and noise ratio of 3. The sensing performance of the cobalt oxide puffy balls/GC sensor is compared in Table 1. The high sensitivity is due to the large

surface area to volume ratio and p-type semiconducting nature of puffy balls-like cobalt oxide nanostructures [36,37].

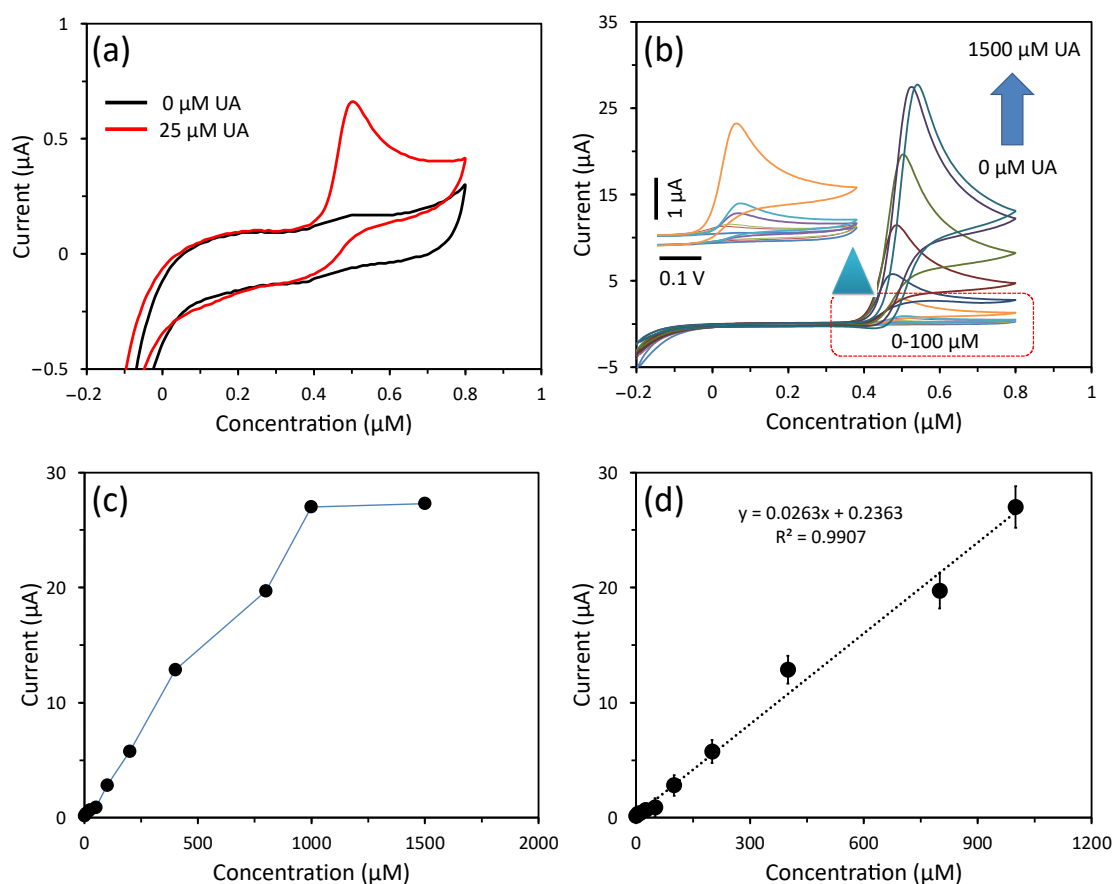


**Figure 5.** (a) CV response of cobalt oxide puffy balls/GC sensor towards 0  $\mu\text{M}$  and 25  $\mu\text{M}$  UA concentration and (b) CV response for 0 to 1500  $\mu\text{M}$  UA concentration in PBS buffer (pH = 7.4). (c) current response vs. UA concentration plot, and (d) calibrated plot showing slope (0.0263  $\mu\text{A}/\mu\text{M}$ ) and regression coefficient ( $R^2$ ) of 0.9907. Inset b presents CV response at a low-concentration range (0 to 100  $\mu\text{M}$ ) of UA.

**Table 1.** Comparison of electrochemical non-enzymatic UA sensing performance of cobalt oxide puffy balls/GC sensor with previously published literature.

Modified Electrode	Sensing Method	Detection Range ( $\mu\text{M}$ )	Limit of Detection ( $\mu\text{M}$ )	Sensitivity ( $\mu\text{Acm}^{-2}\text{mM}^{-1}$ )	Ref.
g- $\text{C}_3\text{N}_4$ NSs/GCE	DPV	100–1000	4.45	-	[7]
Ag- $\text{Fe}_2\text{O}_3$ @PANI	DPV	0.001–0.90	0.000102	128290	[21]
Au/RGO/GCE	DPV	8.8–53	1.8	-	[22]
Cubic Pd/RGO/GCE	DPV	4–469.5	1.6	-	[23]
RGO/PB 100/GCE	CV	40–415	8.0	-	[24]
PCN/MWCNT/GCE	DPV	0.2–20	0.139	-	[25]
B-MWCNT/GCE	CV	60–250	0.65	-	[26]
PtNi@ $\text{MoS}_2$ NSs/GCE	DPV	0.5–600	0.1	-	[27]
Cysteic acid/GCE	DPV	1.0–19	0.36	-	[28]

Table 1. Cont.

Modified Electrode	Sensing Method	Detection Range ( $\mu\text{M}$ )	Limit of Detection ( $\mu\text{M}$ )	Sensitivity ( $\mu\text{Acm}^{-2}\text{mM}^{-1}$ )	Ref.
PPy-CB-Co <sub>3</sub> O <sub>4</sub> /GCE	CV	0.75–305	0.46	0.8786	[30]
Cu <sub>2</sub> O/ferrocene/uricase/GCE	DPV	0.1–1000	0.0596	1.9	[33]
Co <sub>3</sub> O <sub>4</sub> nano berries/GCE	CV	5–3000	2.4	206	[36]
Co <sub>3</sub> O <sub>4</sub> porous NSs/GCE	CV	0–2500	10	470	[37]
Silky Co <sub>3</sub> O <sub>4</sub> nanomaterial/GCE	CV	500–3500	100	-	[46]
MnO <sub>2</sub> NFs/NG/GCE	SDLSV	10–100	0.039	-	[47]
Co <sub>3</sub> O <sub>4</sub> puffy balls/GCE	CV	0–1000	2.4	307	This work
Co <sub>3</sub> O <sub>4</sub> puffy balls/GCE	DPV	0–1500	1.6	2158	This work

Abbreviations: Graphitic carbon nitride—g-C<sub>3</sub>N<sub>4</sub>; nanosheets—NSs; glassy carbon electrode—GCE; gold—Au; differential pulse voltammetry—DPV; silver—Ag; iron oxide—Fe<sub>2</sub>O<sub>3</sub>; polyaniline—PANI; reduced graphene oxide—RGO; palladium—Pd; Prussian blue—PB; cyclic voltammetry—CV; porous carbon nitride—PCN; multi-wall carbon nanotube—MWCNT; platinum—Pt; nickel—Ni; molybdenum disulfide—MoS<sub>2</sub>; polypyrrole—Ppy; carbon black—CB; cobalt oxide—Co<sub>3</sub>O<sub>4</sub>; cuprous oxide—Cu<sub>2</sub>O; manganese dioxide—MnO<sub>2</sub>; nanoflowers—NFs; nitrogen-doped graphene—NG; second-derivative linear sweep voltammetry—SDLSV.

### 3.4. Detection of UA Using DPV

DPV is a pulsed technique in which ramp voltage is applied. Due to the short sampling time of applied ramp voltage in DPV, the capacitive charging current is minimized compared to the Faradaic current, and the ratio of Faradaic current to non-Faradaic current increases, which makes DPV more sensitive compared to the CV technique [32]. In addition, DPV accurately accounts for double-layer capacitance in which changes occur even when a small molecule of analyte absorbs at the electrode surface with pulse sampling. In contrast, CV suffers from excessive capacitance changes [33,46]. Therefore, we utilized the DPV technique to detect UA.

Figure 6 depicts the measured DPV and calibration curves for different UA concentrations (0 mM to 2 mM) in the 0.2 V to 0.7 V voltage range. The cobalt oxide puffy balls/GC sensor responded in the presence of UA in the buffer due to UA oxidation (Figure 6a). In addition, the DPV oxidation current increased with UA concentration (Figure 6b).

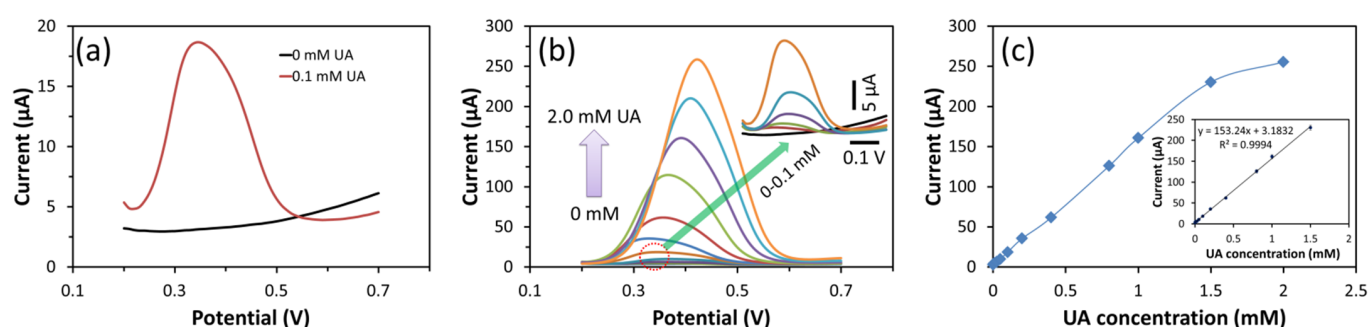


**Figure 6.** DPV response of cobalt oxide puffy balls/GC sensor towards 0 mM and 0.1 mM UA (a), from 0 to 2.0 mM UA in PBS buffer (pH = 7.4) (b), and current response vs. UA concentration plot (c). Inset b is the DPV response at a low-concentration range (0 to 0.1 mM) of UA. Inset c represents the calibrated plot showing a slope (153.24  $\mu\text{A}/\text{mM}$ ) and  $R^2$  of 0.9994.

A linear increase in current is observed with increasing UA concentration up to 1.5 mM (Figure 6c). Further from the obtained calibration plot, the cobalt oxide puffy balls/GC sensor resulted in high sensitivity of 2158  $\mu\text{A}/\text{mM}\cdot\text{cm}^2$ , which is ~6 times more sensitive towards UA compared to the CV-based sensitivity of cobalt oxide puffy balls/GC sensor (Table 1). This high sensitivity of the fabricated sensor is attributed to nanostructure



morphology that offers more active sites available at the surface of puffy balls and the p-type semiconduction nature of cobalt oxide.

### 3.5. Selectivity, Stability, and Reproducibility Tests

Selectivity, long-term stability, and fabrication reproducibility are significant factors for any sensor. To investigate the selectivity of the electrochemical non-enzymatic cobalt oxide puffy balls/GC sensor, the CV scans were recorded in buffer containing (i) 50  $\mu\text{M}$  UA only, (ii) 50  $\mu\text{M}$  UA, and 50  $\mu\text{M}$  of each possible interfering species (i.e., urea, sodium chloride, fructose, glucose, potassium chloride, L-cysteine, and lactic acid), and (iii) 50  $\mu\text{M}$  UA, and 100  $\mu\text{M}$  of each above-interfering species (Figure 7a). The sensor showed a slightly positive CV current response in interfering species' presence at high concentrations. Additionally, the long-term stability of the cobalt oxide puffy balls/GC sensor was evaluated for 10 weeks (Figure 7b). From the obtained CV response curves (Figure 7b), the calibrated histogram shows that the sensor holds its initial response of  $\sim 93.3\%$ , which confirms the high storage stability of the sensors (Figure 7c). After checking the response towards UA, the sensor was rinsed in PBS buffer, dried, and kept in a desiccator.

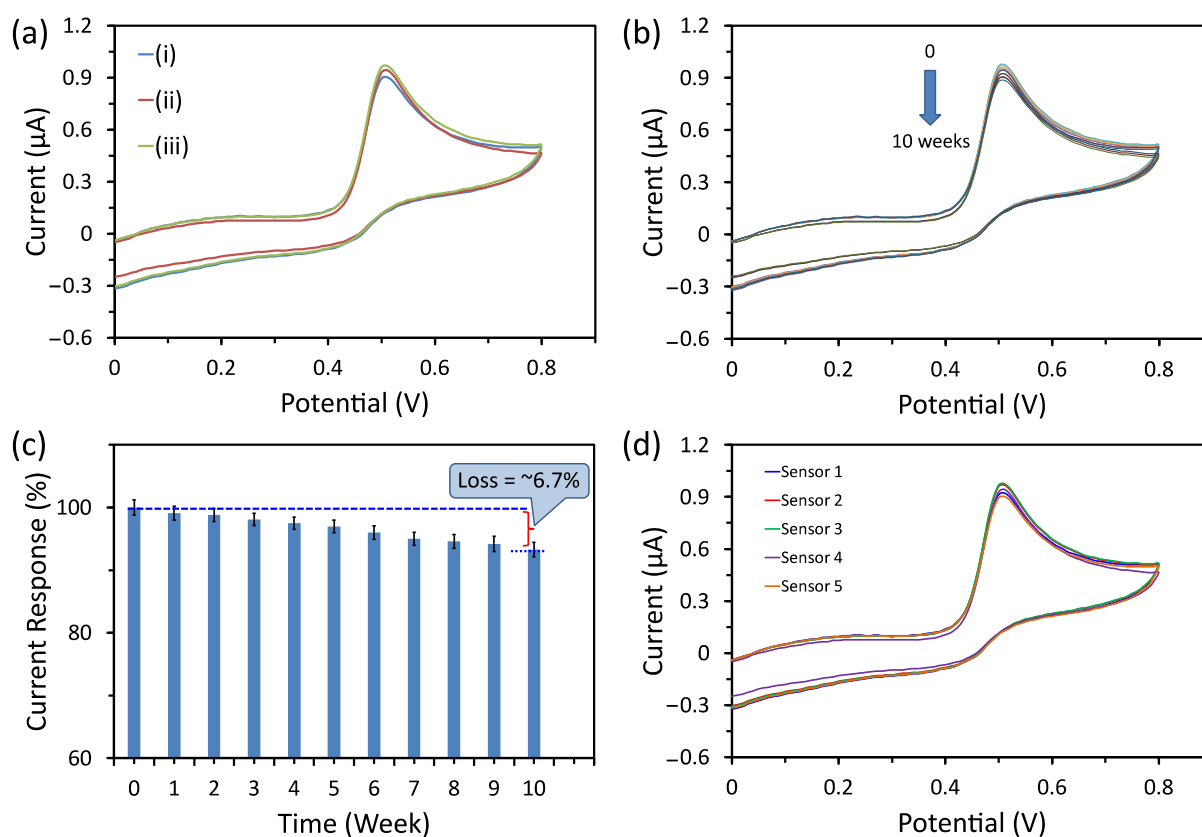


**Figure 7.** (a) CV scans of cobalt oxide puffy balls/GC sensor in PBS buffer containing (i) 50  $\mu\text{M}$  UA only, (ii) 50  $\mu\text{M}$  UA and 50  $\mu\text{M}$  of each possible interfering species (i.e., urea, sodium chloride, fructose, glucose, potassium chloride, L-cysteine, and lactic acid), and (iii) 50  $\mu\text{M}$  UA and 100  $\mu\text{M}$  of each above-interfering species. (b) Sensing response of cobalt oxide puffy balls/GC sensor towards 50  $\mu\text{M}$  UA for 10 weeks storage time. (c) Calibrated response of the sensor showing  $\sim 6.7\%$  decrease compared to the sensor fabricated on day 1. (d) CV scans of five similar fabricated cobalt oxide puffy balls/GC sensors in PBS buffer containing 50  $\mu\text{M}$  UA.

To prevent possible fouling of the electrode. Finally, we checked the fabrication reproducibility of the cobalt oxide puffy balls/GC sensors by fabricating five sensors using the same fabrication protocols. The CV response of all five cobalt oxide puffy balls/GC sensors was tested in the PBS buffer containing 50  $\mu\text{M}$  UA (Figure 7d). A low relative standard deviation (RSD) of 3.6% indicates good fabrication reproducibility.

### 3.6. UA Detection in Serum Sample

To evaluate the applicability of the fabricated cobalt oxide puffy balls/GC sensor for UA detection in serum samples (H4522; Sigma-Aldrich, Saint Louis, MO, USA), we employed a standard addition-based method. First, a known concentration of UA (i.e., 50, 100, and 200  $\mu\text{M}$ ) was added to the serum sample, and total UA concentration was estimated using cobalt oxide puffy balls/GC sensor. From the measurement results, recovery (%) and RSD (%) were estimated (Table 2). The results indicate good recovery and low RSD, which confirms the suitability of the cobalt oxide puffy balls/GC sensor for detecting UA in real samples.

**Table 2.** UA analysis in human serum (H4522) sample using fabricated cobalt oxide puffy balls/GC sensor.

Sample	Added UA ( $\mu\text{M}$ )	Found UA ( $\mu\text{M}$ )	Recovery (%)	RSD (%) ( $n = 3$ )
Human serum (H4522)	0	280	-	-
	50	328.7	97.4	3.1
	100	196.6	96.6	2.8
	200	391.6	95.8	3.4

## 4. Conclusions

In summary, we synthesized puffy balls-like cobalt oxide nanostructures using the hydrothermal method and characterized their crystal structure and surface morphology using different techniques (i.e., XRD and FESEM). The non-enzymatic electrochemical UA sensor was designed with as-synthesized puffy balls-like cobalt oxide nanostructures. The sensing performance of fabricated cobalt oxide puffy balls/GC sensor was tested for UA detection using two techniques (i.e., CV and DPV), and their sensing performance was compared. The fabricated cobalt oxide puffy balls/GC sensor exhibited high sensitivity towards UA, which is  $\sim 6$  times more sensitive when measured using the DPV technique ( $2158 \mu\text{A}/\text{mM}\cdot\text{cm}^2$ ) compared to the sensitivity obtained with CV ( $370 \mu\text{A}/\text{mM}\cdot\text{cm}^2$ ). Additionally, the cobalt oxide puffy balls/GC sensor showed good selectivity, long-term stability, fabrication reproducibility, and applicability in the human serum sample. The puffy balls-shaped cobalt oxide nanostructure with a high surface area can be an exciting working electrode nanomaterial for fabricating different sensors using a specific enzyme/other metal or metal oxide modifications.

**Author Contributions:** Conceptualization, V.N., S.M. and R.A.; methodology, S.M. and V.N.; software, S.M. and M.K.; validation, S.M., V.N. and M.K.; formal analysis, V.N. and M.K.; resources, R.A.; writing—original draft preparation, S.M. and V.N.; writing—review and editing, R.A., S.A., K.S.B., A.A., M.B.A., S.M.N., P.M. and A.K.; supervision, R.A.; funding acquisition, R.A. All authors have read and agreed to the published version of the manuscript.

**Funding:** R.A. gratefully acknowledges the Ramalingaswami Fellowship Award (BT/RLF/Re-entry/28/2018) and research funding from the Department of Biotechnology (DBT), Government of India. This study is supported via funding from Prince Sattam Bin Abdulaziz University project number (PSAU/2023/R/1444). Also, SM and MK would like to thank the Ministry of Education, Government of India, for the Prime Minister’s Research Fellows (PMRF) award.

**Institutional Review Board Statement:** Not applicable.

**Informed Consent Statement:** Not applicable.

**Data Availability Statement:** Not applicable.

**Conflicts of Interest:** The authors declare no conflict of interest.

## References

1. Dai, X.; Fang, X.; Zhang, C.; Xu, R.; Xu, B. Determination of Serum Uric Acid Using High-Performance Liquid Chromatography (HPLC)/Isotope Dilution Mass Spectrometry (ID-MS) as a Candidate Reference Method. *J. Chromatogr. B Analyt. Technol. Biomed. Life Sci.* **2007**, *857*, 287–295. [[CrossRef](#)]
2. Rock, K.L.; Kataoka, H.; Lai, J.J. Uric Acid as a Danger Signal in Gout and Its Comorbidities. *Nat. Rev. Rheumatol.* **2013**, *9*, 13–23. [[CrossRef](#)] [[PubMed](#)]
3. Soltani, Z.; Rasheed, K.; Kapusta, D.R.; Reisin, E. Potential Role of Uric Acid in Metabolic Syndrome, Hypertension, Kidney Injury, and Cardiovascular Diseases: Is It Time for Reappraisal? *Curr. Hypertens. Rep.* **2013**, *15*, 175–181. [[CrossRef](#)]
4. Alderman, M.; Aiyer, K.J.V. Uric Acid: Role in Cardiovascular Disease and Effects of Losartan. *Curr. Med. Res. Opin.* **2004**, *20*, 369–379. [[CrossRef](#)]
5. Leiba, A.; Vinker, S.; Dinour, D.; Holtzman, E.J.; Shani, M. Uric Acid Levels Within the Normal Range Predict Increased Risk of Hypertension: A Cohort Study. *J. Am. Soc. Hypertens.* **2015**, *9*, 600–609. [[CrossRef](#)] [[PubMed](#)]
6. King, C.; Lanaspas, M.A.; Jensen, T.; Tolan, D.R.; Sanchez-Lozada, L.G.; Johnson, R.J. Uric Acid in Chronic Kidney Disease. *Contrib. Nephrol.* **2018**, *192*, 88–102. [[PubMed](#)]
7. Murugan, N.; Chan-Park, M.B.; Sundramoorth, A.K. Electrochemical Detection of Uric Acid on Exfoliated Nanosheets of Graphitic-Like Carbon Nitride ( $g\text{-C}_3\text{N}_4$ ) Based Sensor. *J. Electrochem. Soc.* **2019**, *166*, B3163–B3170. [[CrossRef](#)]
8. Ahmad, R.; Wolfbeis, O.S.; Hahn, Y.-B.; Alshareef, H.N.; Torsi, L.; Salama, K.N. Deposition of Nanomaterials: A Crucial Step in Biosensor Fabrication. *Mater. Today Commun.* **2018**, *17*, 289–321. [[CrossRef](#)]
9. Ahmad, R.; Tripathy, N.; Jang, N.K.; Khang, G.; Hahn, Y.-B. Fabrication of Highly Sensitive Uric Acid Biosensor based on Directly Grown ZnO Nanosheets on Electrode Surface. *Sens. Actuators B Chem.* **2015**, *206*, 146–151. [[CrossRef](#)]
10. Zhang, W.; Zhao, X.; Diao, L.; Li, H.; Tong, Z.; Gu, Z.; Miao, B.; Xu, Z.; Zhang, H.; Wu, Y.; et al. Highly Sensitive Uric Acid Detection Based on a Graphene Chemoresistor and Magnetic Beads. *Biosensors* **2021**, *11*, 304. [[CrossRef](#)]
11. Ahmad, R.; Tripathy, N.; Ahn, M.-S.; Hahn, Y.-B. Solution Process Synthesis of High Aspect Ratio ZnO Nanorods on Electrode Surface for Sensitive Electrochemical Detection of Uric Acid. *Sci. Rep.* **2017**, *7*, 46475. [[CrossRef](#)] [[PubMed](#)]
12. Hassan, M.H.; Vyas, C.; Grieve, B.; Bartolo, P. Recent Advances in Enzymatic and Non-Enzymatic Electrochemical Glucose Sensing. *Sensors* **2021**, *21*, 4672. [[CrossRef](#)]
13. Ahmad, R.; Mahmoudi, T.; Ahn, M.-S.; Hahn, Y.-B. Recent Advances in Nanowires-Based Field-Effect Transistors for Biological Sensor Applications. *Biosens. Bioelectron.* **2018**, *100*, 312–325. [[CrossRef](#)] [[PubMed](#)]
14. Tung, T.T.; Nine, M.J.; Krebsz, M.; Pasinszki, T.; Coghlan, C.J.; Tran, D.N.H.; Losic, D. Recent Advances in Sensing Applications of Graphene Assemblies and Their Composites. *Adv. Funct. Mater.* **2017**, *27*, 1702891. [[CrossRef](#)]
15. Pasinszki, T.; Krebsz, M.; Tung, T.T.; Losic, D. Carbon Nanomaterial Based Biosensors for Non-Invasive Detection of Cancer and Disease Biomarkers for Clinical Diagnosis. *Sensors* **2017**, *17*, 1919. [[CrossRef](#)] [[PubMed](#)]
16. Zhu, Y.; Tian, Q.; Li, X.; Wu, L.; Yu, A.; Lai, G.; Fu, L.; Wei, Q.; Dai, D.; Jiang, N.; et al. A Double-Deck Structure of Reduced Graphene Oxide Modified Porous  $\text{Ti}_3\text{C}_2\text{T}_x$  Electrode towards Ultrasensitive and Simultaneous Detection of Dopamine and Uric Acid. *Biosensors* **2021**, *11*, 462. [[CrossRef](#)]
17. Li, G.; Wu, J.; Qi, X.; Wan, X.; Liu, Y.; Chen, Y.; Xu, L. Molecularly Imprinted Polypyrrole Film-Coated Poly(3,4-ethylenedioxythiophene):Polystyrene Sulfonate-Functionalized Black Phosphorene for the Selective and Robust Detection of Norfloxacin. *Mater. Today Chem.* **2022**, *26*, 101043. [[CrossRef](#)]
18. Li, G.; Qi, X.; Zhang, G.; Wang, S.; Li, K.; Wu, J.; Wan, X.; Liu, Y.; Li, Q. Low-cost Voltammetric Sensors for Robust Determination of Toxic Cd(II) and Pb(II) in Environment and Food Based on Shuttle-like  $\alpha\text{-Fe}_2\text{O}_3$  Nanoparticles Decorated  $\beta\text{-Bi}_2\text{O}_3$  Microspheres. *Microchem. J.* **2022**, *179*, 107515. [[CrossRef](#)]
19. Lee, W.-C.; Kim, K.-B.; Gurudatt, N.G.; Hussain, K.K.; Choi, C.S.; Park, D.-S.; Shim, Y.-B. Comparison of Enzymatic and Non-Enzymatic Glucose Sensors Based on Hierarchical Au-Ni Alloy with Conductive Polymer. *Biosens. Bioelectron.* **2019**, *130*, 48–54. [[CrossRef](#)]
20. Khan, M.; Nagal, V.; Nakate, U.T.; Khan, M.R.; Khosla, A.; Ahmad, R. Engineered CuO Nanofibers with Boosted Nonenzymatic Glucose Sensing Performance. *J. Electrochem. Soc.* **2021**, *168*, 067507. [[CrossRef](#)]
21. Ponnaiah, S.K.; Periakaruppan, P.; Vellaichamy, B. New Electrochemical Sensor Based on a Silver-Doped Iron Oxide Nanocomposite Coupled with Polyaniline and Its Sensing Application for Picomolar Level Detection of Uric Acid in Human Blood and Urine Samples. *J. Phys. Chem. B* **2018**, *122*, 3037–3046. [[CrossRef](#)] [[PubMed](#)]
22. Wang, C.; Du, J.; Wang, H.; Zou, C.E.; Jiang, F.; Yang, P.; Du, Y. A Facile Electrochemical Sensor Based on Reduced Graphene Oxide and Au Nanoplates Modified Glassy Carbon Electrode for Simultaneous Detection of Ascorbic Acid, Dopamine and Uric Acid. *Sens. Actuators B* **2014**, *204*, 302–309. [[CrossRef](#)]

23. Wang, J.; Yang, B.; Zhong, J.; Yan, B.; Zhang, K.; Zhai, C.; Shiraishi, Y.; Du, Y.; Yang, P. Dopamine and Uric Acid Electrochemical Sensor Based on a Glassy Carbon Electrode Modified with Cubic Pd and Reduced Graphene Oxide Nanocomposite. *J. Colloid Interface Sci.* **2017**, *497*, 172–180. [[CrossRef](#)]
24. Santos, P.L.D.; Katic, V.; Toledo, K.C.; Bonacin, J.A. Photochemical One-Pot Synthesis of Reduced Graphene Oxide/Prussian Blue Nanocomposite for Simultaneous Electrochemical Detection of Ascorbic Acid, Dopamine, and Uric Acid. *Sens. Actuators B Chem.* **2018**, *255*, 2437. [[CrossRef](#)]
25. Lv, J.; Li, C.; Feng, S.; Chen, S.-M.; Ding, Y.; Chen, C.; Hao, Q.; Yang, T.-H.; Lei, W. A Novel Electrochemical Sensor for Uric Acid Detection Based on PCN/MWCNT. *Ionics* **2019**, *25*, 4437–4445. [[CrossRef](#)]
26. Tsierkezos, N.G.; Ritter, U.; Thaha, Y.N.; Downing, C.; Szroeder, P.; Scharff, P. Multi-Walled Carbon Nanotubes Doped with Boron as an Electrode Material for Electrochemical Studies on Dopamine, Uric Acid, and Ascorbic Acid. *Microchim. Acta* **2016**, *183*, 35–47. [[CrossRef](#)]
27. Ma, L.; Zhang, Q.; Wu, C.; Zhang, Y.; Zeng, L. PtNi Bimetallic Nanoparticles Loaded MoS<sub>2</sub> Nanosheets: Preparation and Electrochemical Sensing Application for the Detection of Dopamine and Uric Acid. *Anal. Chim. Acta* **2019**, *1055*, 17–25. [[CrossRef](#)]
28. Hassanvand, Z.; Jalali, F. Simultaneous Determination of IDOPA, L-tyrosine and Uric Acid by Cysteic Acid-Modified Glassy Carbon Electrode. *Mater. Sci. Eng. C* **2019**, *98*, 496–502. [[CrossRef](#)]
29. Turkkan, G.; Bas, S.Z.; Atacan, K.; Ozmen, M. An Electrochemical Sensor based on a Co<sub>3</sub>O<sub>4</sub>-ERGO Nanocomposite Modified Screen-Printed Electrode for Detection of Uric Acid in Artificial Saliva. *Anal. Methods* **2022**, *14*, 67–75. [[CrossRef](#)]
30. Ahmed, J.; Faisal, M.; Alsareii, S.A.; Harraz, F.A. Highly Sensitive and Selective Non-Enzymatic Uric Acid Electrochemical Sensor Based on Novel Polypyrrole-Carbon Black-Co<sub>3</sub>O<sub>4</sub> Nanocomposite. *Adv. Compos. Hybrid Mater.* **2022**, *5*, 920–933. [[CrossRef](#)]
31. Nagal, V.; Kumar, V.; Khan, M.; Alomar, S.; Tripathy, N.; Singh, K.; Khosla, A.; Ahmad, N.; Hafiz, A.K.; Ahmad, R. A Highly Sensitive Uric Acid Biosensor Based on Vertically Arranged ZnO Nanorods on ZnO Nanoparticles Seeded Electrode. *New J. Chem.* **2021**, *45*, 18863–18870. [[CrossRef](#)]
32. Arvand, M.; Hassannezhad, M. Magnetic Core-Shell Fe<sub>3</sub>O<sub>4</sub>@SiO<sub>2</sub>/MWCNT Nanocomposite Modified Carbon Paste Electrode for Amplified Electrochemical Sensing of Uric Acid. *Mater. Sci. Eng. C* **2014**, *36*, 160–167. [[CrossRef](#)] [[PubMed](#)]
33. Yan, Q.; Zhi, N.; Yang, L.; Xu, G.; Feng, Q.; Zhang, Q.; Sun, S. A Highly Sensitive Uric Acid Electrochemical Biosensor based on a Nano-Cube Cuprous Oxide/Ferrocene/Uricase Modified Glassy Carbon Electrode. *Sci. Rep.* **2020**, *10*, 10607. [[CrossRef](#)]
34. Bhat, K.S.; Ahmad, R.; Mahmoudi, T.; Hahn, Y.-B. High Performance Chemical Sensor with Field-Effect Transistors Array for Selective Detection of Multiple Ions. *Chem. Eng. J.* **2021**, *417*, 128064. [[CrossRef](#)]
35. Chang, A.S.; Tahira, A.; Chang, F.; Solangi, A.G.; Bhatti, M.A.; Vigolo, B.; Nafady, A.; Ibupoto, Z.H. Highly Heterogeneous Morphology of Cobalt Oxide Nanostructures for the Development of Sensitive and Selective Ascorbic Acid Non-Enzymatic Sensor. *Biosensors* **2023**, *13*, 147. [[CrossRef](#)] [[PubMed](#)]
36. Nagal, V.; Tuba, T.; Kumar, V.; Alam, S.; Ahmad, A.; Alshammari, M.B.; Hafiz, A.K.; Ahmad, R. A Non-Enzymatic Electrochemical Sensor Composed of Nano-Berry Shaped Cobalt Oxide Nanostructures on a Glassy Carbon Electrode for Uric Acid Detection. *New J. Chem.* **2022**, *46*, 12333–12341. [[CrossRef](#)]
37. Masrat, S.; Nagal, V.; Khan, M.; Moid, I.; Alam, S.; Bhat, K.S.; Khosla, A.; Ahmad, R. Electrochemical Ultrasensitive Sensing of Uric Acid on Non-Enzymatic Porous Cobalt Oxide Nanosheets-Based Sensor. *Biosensors* **2022**, *12*, 1140. [[CrossRef](#)]
38. Nagal, V.; Khan, M.; Masrat, S.; Alam, S.; Ahmad, A.; Alshammari, M.B.; Bhat, K.S.; Ahmad, R. Hexagonal Cobalt Oxide Nanosheet-Based Enzymeless Electrochemical Uric Acid Sensor with Improved Sensitivity. *New J. Chem.* **2023**, *47*, 4206–4212. [[CrossRef](#)]
39. Kogularasu, S.; Govindasamy, M.; Chen, S.-M.; Akilarasan, M.; Mani, V. 3D graphene Oxide-Cobalt Oxide Polyhedrons for Highly Sensitive Non-Enzymatic Electrochemical Determination of Hydrogen Peroxide. *Sens. Actuators B Chem.* **2017**, *253*, 773–783. [[CrossRef](#)]
40. Zhang, H.; Liu, S. A Combined Self-Assembly and Calcination Method for Preparation of Nanoparticles-Assembled Cobalt Oxide Nanosheets using Graphene Oxide as Template and their Application for Non-Enzymatic Glucose Biosensing. *J. Colloid Interface Sci.* **2017**, *485*, 159–166. [[CrossRef](#)]
41. Kang, L.; He, D.; Bie, L.; Jiang, P. Nanoporous Cobalt Oxide Nanowires for Non-Enzymatic Electrochemical Glucose Detection. *Sens. Actuators B Chem.* **2015**, *220*, 888–894. [[CrossRef](#)]
42. Mondal, S.; Madhuri, R.; Sharma, P.K. Probing the Shape Specific Electrochemical Properties of Cobalt Oxide Nanostructures for their Application as Selective and Sensitive Nonenzymatic Glucose Sensors. *J. Mater. Chem. C* **2017**, *5*, 6497–6505. [[CrossRef](#)]
43. Chang, A.S.; Memon, N.N.; Amin, S.; Chang, F.; Aftab, U.; Abro, M.I.; Chandio, A.; Shah, A.A.; Ibupoto, M.H.; Ansari, M.A.; et al. Facile Non-Enzymatic Lactic Acid Sensor based on Cobalt Oxide Nanostructures. *Electroanalysis* **2019**, *31*, 1296–1303. [[CrossRef](#)]
44. Numan, A.; Duraisamy, N.; Omar, F.S.; Mahipal, Y.K.; Ramesh, K.; Ramesh, S. Enhanced Electrochemical Performance of Cobalt Oxide Nanocube Intercalated Reduced Graphene Oxide for Supercapacitor Application. *RSC Adv.* **2016**, *6*, 34894–34902. [[CrossRef](#)]
45. Hu, F.X.; Hu, T.; Chen, S.; Wang, D.; Rao, Q.; Liu, Y.; Dai, F.; Guo, C.; Yang, H.B.; Li, C.M. Single-Atom Cobalt-Based Electrochemical Biomimetic Uric Acid Sensor with Wide Linear Range and Ultralow Detection Limit. *Nano-Micro Lett.* **2021**, *13*, 7. [[CrossRef](#)]

46. Chang, A.S.; Tahira, A.; Chang, F.; Memon, N.N.; Nafady, A.; Kasry, A.; Ibupoto, Z.H. Silky  $\text{Co}_3\text{O}_4$  Nanostructures for the Selective and Sensitive Enzyme Free Sensing of Uric Acid. *RSC Adv.* **2021**, *11*, 5156–5162. [[CrossRef](#)]
47. Li, Q.; Xia, Y.; Wan, X.; Yang, S.; Cai, Z.; Ye, Y.; Li, G. Morphology-Dependent  $\text{MnO}_2$  Nitrogen-Doped Graphene Nanocomposites for Simultaneous Detection of Trace Dopamine and Uric Acid. *Mater. Sci. Eng. C* **2020**, *109*, 110615. [[CrossRef](#)]

**Disclaimer/Publisher’s Note:** The statements, opinions and data contained in all publications are solely those of the individual author(s) and contributor(s) and not of MDPI and/or the editor(s). MDPI and/or the editor(s) disclaim responsibility for any injury to people or property resulting from any ideas, methods, instructions or products referred to in the content.